

Atmospheric monitoring with an infrared radiometer

M.K. Daniel^{1,a} and P.M. Chadwick^{2,b}

¹ Department of Physics, University of Liverpool, Liverpool L69 8DX, UK

² Department of Physics, University of Durham, Durham DH1 3LE, UK

Abstract. The molecular atmosphere has a number of windows where it is effectively transparent to electromagnetic radiation, one of these being in the infrared 8–14 micron region. The presence of clouds and aerosols, which are more effective emitters of infrared radiation, in the atmosphere show up as an increase in the effective brightness temperature compared to the clear sky. This talk will cover the results from operating a scanning radiometer at the H.E.S.S. site in Namibia in determining atmospheric conditions.

1. Introduction

The infra-red luminosity of the sky (L_{sky}) is actually a collective sum of the emission of a number of different constituent parts

$$L_{\text{sky}} = \epsilon_m \sigma \int T_m^4 + \epsilon_a \sigma \int T_a^4 + \epsilon_{wv} \sigma \int T_{wv}^4 + \epsilon_l \sigma T_{\text{lens}}^4 + \dots$$

where $\int T$ is the relevant integrated temperature profile in the line of sight and ϵ denotes the emissivity of the molecular (m), the aerosol (a), the water vapour (wv) profiles of the atmosphere respectively and with the addition of detector related foreground, i.e. a lens (l), to the radiation budget. The altitude dependent temperature profiles of various representative standard atmospheric models are shown in Fig. 1.

As can be seen in Fig. 2, in the 8–14 μm band the molecular component is a very poor emitter, so the equivalent blackbody temperature of the molecular sky should appear very cold; conversely condensed water is a good approximation of a black body emitter, so cloud consequently makes the sky appear much warmer than in clear sky conditions. As the lowest altitudes are also the warmest these will contribute the most to the observed infrared radiation budget; this also happens to be the region that will be most affected by the varying aerosol concentration making for a sensitive measure of the atmospheric aerosol content for these greybody emitters.

2. Monitoring the atmosphere

In this section we look at the various equivalent sky brightness temperature signatures for different cloud, aerosol and molecular conditions for real astronomical sites.

^a e-mail: michael.daniel@liverpool.ac.uk

^b e-mail: p.m.chadwick@durham.ac.uk

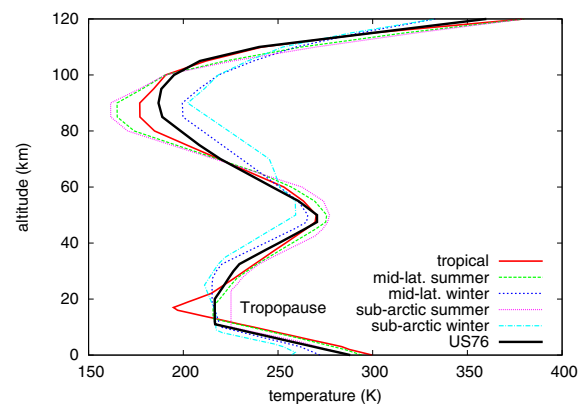


Figure 1. The temperature profile of the atmosphere for various standard models of the MODTRAN simulation package [8].

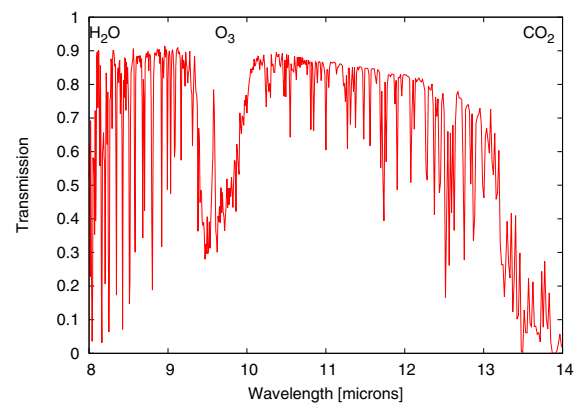


Figure 2. The transmission in the 8–14 μm window for a tropical site at an altitude of 1800 m as calculated by MODTRAN 4 [8].

2.1 Clouds

Figure 3 shows what happens when a cloud passes through the field of view of a Cherenkov telescope¹ (CT) with a paraxially mounted IR radiometer². The cloud shows up as a drop in the trigger rate of the CT and a corresponding increase in the sky brightness temperature.

¹ Here CT6 of HEGRA [1].

² Here a Heitronics model KT19.82 is used.

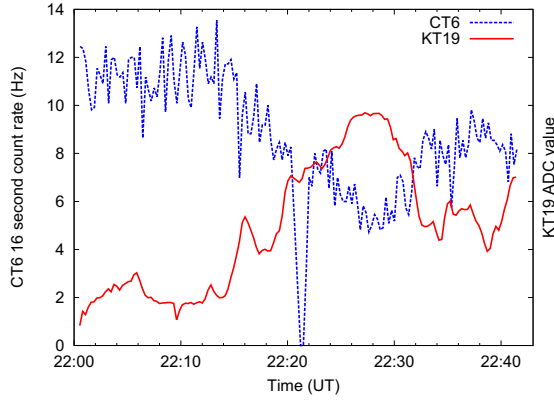


Figure 3. HEGRA CT6 count rate for two observing runs (dashed blue line); KT19 IR radiometer readings for the same runs (solid red line). The dip at $\sim 22:20$ corresponds to a run transition. Adapted from [5].

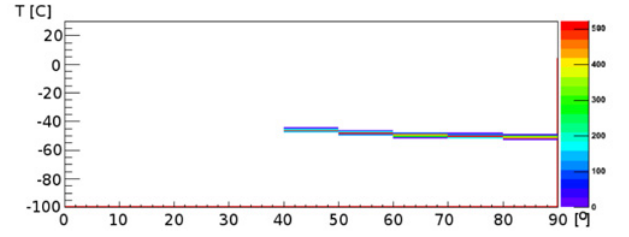
The temperature of the cloud base will be at a similar temperature to the surrounding air. Since the temperature of the atmosphere drops in a linear fashion as a function of altitude (from above the boundary layer at ~ 1 km up to the tropopause at ~ 15 km) then with knowledge of the ground temperature and the temperature lapse rate the cloud temperature can be used as a crude estimator of its altitude (see e.g. [2,3], though as cautioned in [3] these estimates can become unreliable due to reflection of IR light from the ground by low altitude cloud, intervening water vapour, or by changes in the emissivity dependent on the cloud composition (e.g. water droplets versus ice crystals).

2.2 Aerosols

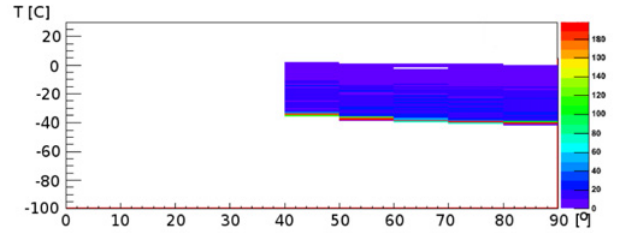
According to [4] the aerosol component can contribute up to 30 Wm^{-2} to the bolometric luminosity of a clear sky. As cloud shows up as a warming of the sky temperature so, too, will the presence of aerosols, albeit to a lesser extent as they are less efficient blackbody emitters³. Figure 4 shows the sky brightness temperature as a function of zenith angle for three different 24 hour periods with very different sky conditions at the H.E.S.S. site⁴. Measurements were taken within a few days of each other, with conditions classified by a Leosphere EZLidar operating simultaneously (see Fig. 5). In Fig. 4a we see the standard observing conditions, for which there is a boundary layer of aerosols up to 2 km above ground and telescope rates and sky brightness temperatures are stable. In Fig. 4b there is a distinct cloud base, which has formed from water condensing on to these aerosols. As the sky is not completely covered the telescope rates are unstable during this time and there is a large increase and variance in the sky brightness temperature also. Figure 4c represents data taken after it has rained, the clouds are

³ Which can mean the difference between a brightness temperature of -56°C or -70°C in the presence or absence of aerosols respectively.

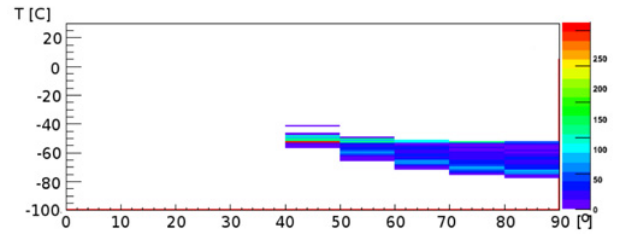
⁴ <https://www.mpi-hd.mpg.de/hfm/HESS/pages/about/site/>



(a) normal conditions with a boundary layer of aerosols to 2 km above ground.

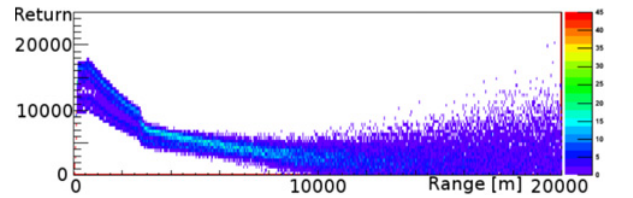


(b) Broken cloud passing through field of view.

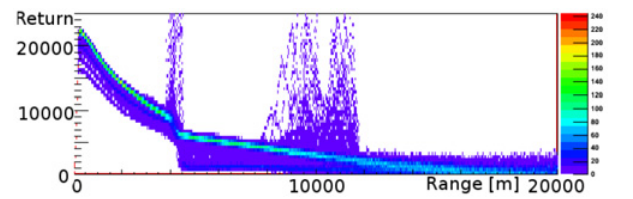


(c) No boundary layer, aerosols have sedimented out of atmosphere.

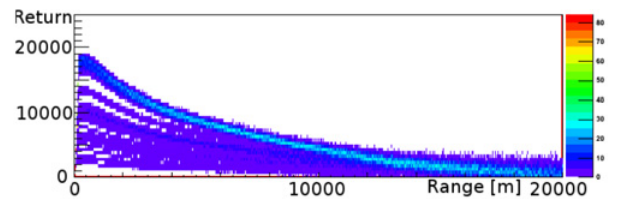
Figure 4. The sky brightness temperature as a function of zenith angle (also known as a skydip) for three different sky conditions.



(a) normal conditions with a boundary layer of aerosols to 2 km above ground.



(b) Broken cloud passing through field of view.



(c) No boundary layer, aerosols have sedimented out of atmosphere.

Figure 5. The range-corrected lidar readings for the data shown in Fig. 4.

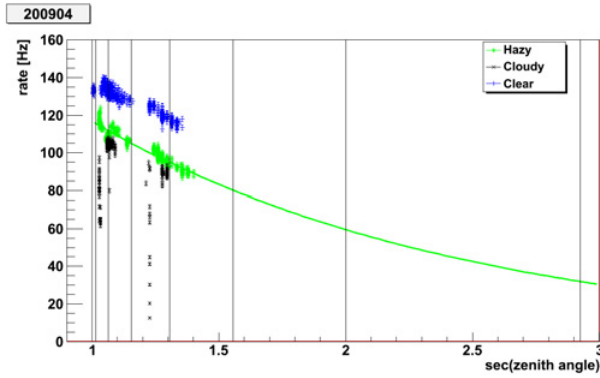


Figure 6. HESS array (3 tel.) trigger rates as a function of zenith angle for the atmospheric conditions in Figs. 4, 5. Green points correspond to normal (4(a)), black points to cloudy (4(b)) and blue points to clear (4(c)) conditions respectively.

gone and the rain has washed the aerosols from the sky. This is an exceptionally clear period during which the boundary layer disappears to below the low altitude limit of the EZLidar (about ~ 500 m) and may even become completely absent. The result is a large variance in the sky brightness temperature which dips to very low values, and there is a correspondingly higher than average telescope trigger rate seen in that night's observations, see Fig. 6.

2.3 Molecules

The molecular component, whilst mostly transparent, will still contribute something to the $8\text{--}14\ \mu\text{m}$ window. In Fig. 7 we see the relative intensity of emission when the water vapour content is varied from 50% to 150% of the standard value for two different model atmospheres (tropical on the left, US Standard 1976 on the right) as calculated by MODTRAN 4. In cold atmospheric conditions the atmosphere cannot hold much water vapour, so there is relatively little variation in the IR emission, whereas the warmer atmospheres (such as near the tropics) can allow a much greater water vapour content, so a variation in the relative humidity becomes much more noticeable as a change in the slope of the emission/temperature as a function of zenith angle.

3. Discussion and conclusions

An infrared radiometer operating in the $8\text{--}14\ \mu\text{m}$ atmospheric window has been shown to be useful for making remote and automatic measurements of clouds and aerosol content. The data for many of the measurements presented are accumulated from both day and night observations. As evidenced in Fig. 4a, there is often very little diurnal variation in the sky brightness temperature⁵ since large temperature swings are limited to the very lowest layers of the atmosphere and seasonal variations

⁵ Except perhaps for the occasional measurement when the sun is in the field of view of the radiometer lens, however these events can be easily accounted for.

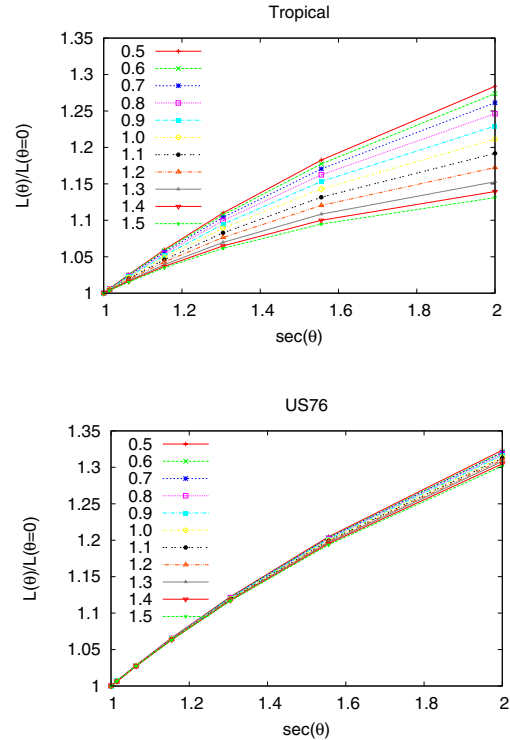


Figure 7. Varying the water vapour content from $0.5\times$ to $1.5\times$ the default for two different model atmospheres: tropical on the top and US Standard on the bottom. Adapted from [5].

that affect the upper atmosphere are long timescale. This demonstrates that daytime observations with a radiometer can be used to forecast that night's observing conditions; an enhanced boundary layer reading could even be used to predict if cloud is likely to form in the next few days. With appropriate study a particular site could be empirically characterised and IR measurements would then be a useful tool for informed advance scheduling of observations. The beginnings of such a study are summarised in [6, 7].

An IR radiometer and a lidar used together make for a very good matched set of instruments for an atmospheric monitoring programme. Estimating cloud height from the sky brightness temperature is possible with knowledge of the screen temperature and the temperature lapse rate, but still has sufficient uncertainty (e.g. from unknown contributions of reflection and the cloud emissivity) that it will never be as accurate or reliable as lidar measurements. As aerosol concentrations are greatest close to the ground, where the temperature is also the greatest, then IR radiometer measurements are a great complement to lidar measurements, since this will be the region that a lidar will not be at maximum efficiency due to geometrical considerations of the overlap between laser beam and the collecting optics. In addition, because an IR radiometer is a passive instrument it will not cause any interference with any observations by surrounding instruments in the same way that firing a laser beam can, making it very useful for independently measuring the atmospheric clarity simultaneously with any astronomical observations.

References

- [1] G. Pühlhofer et al, *Astroparticle Physics* **20**, 267 (2003)
- [2] D.J. Buckley et al, *Experimental Astronomy* **9**, 237 (1999)
- [3] D. Riordan et al, *Journal of Geophysical Research* **110**, 3207 (2005)
- [4] G.J. Dalrymple & M.H. Unsworth, *Quarterly Journal of the Royal Meteorological Society* **104**, 989 (1978)
- [5] M.K. Daniel, Ph.D. thesis, University of Durham (2002); <http://etheses.dur.ac.uk/3840/>
- [6] M.K. Daniel, Y.T.E. Lo & P.M. Chadwick, [arXiv:1402.4739] (2014)
- [7] J. Hahn et al, *Astroparticle Physics* **54**, 25 (2014)
- [8] <http://www.ontar.com/software> (MODTRAN)